# Small-angle neutron scattering measurements of hydrogen and deuterium trapping at dislocations in deformed single-crystalline Pd at low temperature

Brent J. Heuser and Hyunsu Ju

Phys. Rev. B **83**, 094103 — Published 4 March 2011

DOI: 10.1103/PhysRevB.83.094103

# SMALL-ANGLE NEUTRON SCATTERING MEASUREMENTS OF HYDROGEN AND DEUTERIUM TRAPPING AT DISLOCATIONS IN DEFORMED SINGLE CRYSTAL PD AT LOW TEMPERATURE

Brent J. HEUSER and Hyunsu JU

University of Illinois at Urbana-Champaign

Department of Nuclear, Plasma, and Radiological Engineering

Urbana, IL 61801

Abstract

Small-angle neutron scattering (SANS) measurements of hydrogen and deuterium trapped at dislocation defects in deformed single crystal Pd have been performed at 15K, 100K, and 200 K at total interstitial solute concentrations of order $10^{-3}$. This work supports recent incoherent inelastic neutron scattering measurements of the vibrational density of states of trapped hydrogen under similar concentration-temperature conditions [Heuser *et al*., *Phys. Rev. B*, **78** 214101 (2008)]. The measured net absolute macroscopic differential scattering cross sections have been fit with a cylindrical form factor representing solute-decorated dislocation line segments. Generally, very little difference in the measured cross sections was observed with temperature for a given solute type, while a significant change was observed between hydrogen- and deuterium-loaded samples. The latter difference is understood within a cross section model that takes into account the local lattice dilatation associated with solute segregation at dislocations. The application of the model cross section to the net $PdH_{0.0013}$ SANS response yields an effective trapping radius of $R$~10Å and dislocation density of $\rho_d \sim 10^{10}$ cm$^{-2}$. Analysis of the SANS response allowed the local trapped solute concentration (~0.5 [H]/[Pd]) and volumetric dilatation ($\Delta v/\Omega$~1.1) to be determined with the constraint that the system locally satisfies the known lattice expansion of Pd hydride (i.e., Vegard's law).

Keywords: SANS, palladium, hydrogen, dislocation, trapping, Vegard's law

## 1. Introduction

The use of small-angle neutron scattering (SANS) to study hydrogen (deuterium) trapping at dislocations in deformed vanadium was first attempted by Kirchheim *et al.* [1] and Carstanjen *et al.* [2] over twenty years ago. Guinier analysis of these data yielded a trapped segregation radius of $R$~15 Å [1, 2]. SANS measurements of deuterium trapping at dislocations in *deformed Pd* at room temperature and at equilibrium with respect to $D_2$ gas were published by Heuser *et al.* [3]. This work presented a fully-developed analytical cross section model, used single crystal Pd sample material and a hydride cycling procedure that were unique to the published literature at the time. A subsequent publication by Heuser and King [4] presented additional SANS measurements in which differences between cold worked and hydride cycled single crystal Pd were better resolved and analyzed. In the previous work by Heuser *et al.* and by Heuser and King, as well as the current work, the solute-*edge dislocation* trapping interaction is assumed to be responsible for the SANS response. This is consistent with screw dislocations having, to first order, zero hydrostatic strain. More recently Maxelon *et al.* have performed SANS measurements of both hydrogen and deuterium trapping at dislocations in deformed polycrystalline Pd [5]. These authors resolved significant differences in the net SANS response for the two solute types and correlated to the difference in the sign of the trapped solute scattering length.

Experimental procedures and a description of the SANS instrument used for this work are presented in the next section. The results are then presented and will include a discussion of the model cross section, which combinations the model originally developed by Heuser *et al.* [3] and the subsequent cross section pre-factor published by Maxelon *et al.* [5]. Analysis of the measured SANS response within the context of Vegard's law for Pd hydride will be given. This will include discussion of the local concentration of the trapped solute for the with-hydrogen and with-deuterium cases.

## 1. Experimental

The Pd single crystal sample used here was taken from the same ingot described previously by Heuser and King [4]; complete details regarding the supplier and growth method of this ingot are contained in Reference 4. The resolution of the weak net SANS signals associated with trapped solutes requires the reduction or elimination of significant background contributions. In particular, the strong Porod scattering from internal interfaces [6] observed at low wave-vector transfer values ($Q<0.03$ Å$^{-1}$) by Maxelon *et al.* [5] is absent in our previous single crystal Pd SANS data [3, 4] and in the measurements presented below. Strong low-Q Porod scattering from polycrystalline Pd was in fact observed prior to Maxelon *et al*. and attributed to the presence of MnO inclusions imaged with transmission electron microscopy [7].

The deformed single crystal Pd sample used here had a [110] face normal (corresponding to the growth direction of the original ingot [4]), was 0.310 cm thick, had a diameter of approximately 1 cm, and a mass of 4.4681 g. This sample was first cold work to ~40% thickness reduction by cross rolling at room temperature. The sample was then further deformed by cycling across the hydride miscibility gap twice at room temperature, a process known to generate dislocation defects [3, 4]. Representative transmission electron microscopy (TEM) images of Pd after cold working and cold working plus hydride cycling are shown in Figure 1. The cellular dislocation substructure characteristic of cold-worked metals is evident in Figure 1a. Subsequent hydride cycling acts to populate the cell interior regions with dislocations (Fig. 1b).

After deformation, both free surfaces of the sample were mechanically polished, with 0.05 μm levigated alumina used as the final step. Hydrogen and deuterium loading was performed by exposure to the respective gas phases at room temperature in a closed volume of approximately 1 liter using a portable gas loading system. The total pressure reduction $\Delta P$ during absorption and final equilibrium pressure $P_{eq}$ were recorded with absolute capacitance manometers with 100-Torr and 1-Torr full scale supplied by MKS Baratron. The SANS measurement routine was as follows. The sample was first loaded *ex situ* with hydrogen to an equilibrium concentration of 0.0013 [H]/[Pd] at room temperature. The corresponding equilibrium $H_2$ gas pressure was $P_{eq}$=0.052 Torr; equilibrium required approximately 24 hours. The enhancement ratio $\alpha$ [4, 8, 9], defined as the ratio of total solute atomic number density $\rho_T$ (determined from $\Delta P$ using the ideal gas law) to the bulk solute number density at equilibrium $\rho_B$ (determined from $P_{eq}$ using Sieverts' law constants for Pd [10]), for this loading was 1.7. Enhancement ratios of 1.2 to 1.4 are typical in deformed Pd at total solute concentrations of order $10^{-2}$ [solute]/[Pd], and attributed to the hydrogen-edge dislocation trapping interaction increasing the local concentration above bulk [3, 4, 8, 9]. However, larger ratios occur at lower concentrations since the amount of trapped solute will be a larger fraction of the total concentration. This is demonstrated in Fig. 2, which presents several *ex situ* measurements of $\alpha$ versus total solute concentration for deformed single crystal Pd at room temperature.

The CG-2 General Purpose SANS instrument at the High Flux Isotope Reactor at Oak Ridge National Laboratory [11] was used for the measurements presented here. The instrument was configured such that the source-to-sample distance was 7270 mm (5 guides inserted), the sample-to-detector distance was 3500 mm, and the incident neutron wavelength was 7.1±1.1 Å ($\Delta\lambda/\lambda$=0.15). The area detector was offset by 200.0 mm to increase high-$Q$ sensitivity. The measured wave-vector transfer range for this configuration was $0.008 \leq Q \leq 0.20$ Å$^{-1}$. The sample was held in a machined hole in a high-purity Al plate. This plate was mounted to the cold finger of a closed-cycle refrigerator (CCR), which was mounted to the CG-2 SANS instrument. The CCR had two sapphire windows to reduce the scattering background at small angles. The beam at the sample was defined by two 8.5 mm Cd apertures attached to the Al mounting plate that sandwiched the sample. A thermocouple mounted to the Al plate recorded the sample temperature. The loaded samples (both hydrogen and deuterium) were transferred from the portable loading system to the CCR and brought to a pressure of $10^{-4}$ Torr within 30 minutes. At this point the CCR was turned on; the subsequent cooling time from room temperature to 200K was 12 minutes. Further cooling to 15K required ~1 hour. Thus, the total time from the removal of the sample from the loading system to the sample reaching a temperature (~200K) at which significant solute diffusion is inhibited is approximately 40 minutes. We estimate very little solute loss (<2% of the total concentration) during this transition time. Hydrogen and deuterium loss during the SANS measurements was minimal as well; for example, the hydrogen diffusivity in Pd at 200 K is ~$5\times10^{-9}$ cm$^2$/s [12], resulting in an unloading time of ~500 hours (representing the time for the concentration to decrease approximately by one factor of $e$).

The $PdH_{0.0013}$ sample was cooled directly from room temperature to 15K and measured sequentially 15K, 100K, and 200K using the CG2 SANS instrument at Oak Ridge National Laboratory. These measurements were performed in a vacuum of $10^{-4}$ to $10^{-5}$ Torr. The measurement time at each temperature was 12 hours. The sample was then heated to room temperature, placed in the portable loading system and out-gassed at 150 ˚C for 9 hours in a vacuum of $10^{-6}$ Torr, forming the zero-concentration deformed reference sample. The zero-concentration deformed reference sample was cooled directly from room temperature to 15K and measured sequentially 15K, 100K, and 200K for 14 hours at each temperature. The sample was then heated to room temperature, transferred to the portable loading system, and loaded with deuterium to an equilibrium concentration of 0.00084 [D]/[Pd]. Equilibrium

required approximately 24 hours. The equilibrium $D_2$ gas pressure was $P_{eq}$=0.197 Torr, corresponding to an enhancement ratio of 2.3. This large enhancement ratio indicates significant solute trapping, confirming that no dislocation defect recovery occurred during the 9 hour 150 ˚C outgassing procedure to remove hydrogen. The $PdD_{0.00084}$ sample was measured at 15K and 100K for 14 hours each. The empty beam (21 hours) and beam blocked background (12 hours) measurements were recorded at room temperature during the out-gassing and deuterium loading procedures. Transmission measurements at each temperature for all three samples ($PdH_{0.0013,}$ $PdD_{0.00084}$, and zero-concentration) were performed. A total of six days of beam time was used.

## 2. Results

The absolute differential macroscopic scattering cross section, $d\Sigma/d\Omega$, for $PdH_{0.0013}$, $PdD_{0.00084}$, and zero-concentration deformed Pd reference samples measured at 15K are shown in Figure 3. These data were corrected for the empty beam and beam block backgrounds, for the sample transmission, and placed on an absolute scale using the PORASIL-A standard. The with-hydrogen response is significantly larger than the with-deuterium response. As mentioned in the Introduction, a large disparity between the with-hydrogen and with-deuterium SANS responses was first reported by Maxelon *et al*. [5]. These authors attributed this observation to the combined effect of local volumetric dilatation associated with solute phase separation at dislocations and the fact that the neutron-nuclear scattering length $b_S$ of hydrogen and deuterium solutes are opposite in sign ($b_H$ = –0.3739 x $10^{-6}$ Å and $b_D$ = 0.6671 x $10^{-6}$ Å). In simple terms, the negative scattering length of trapped hydrogen further increases the scattering length contrast between the hydride-induced lattice expansion at the dislocation defects and the bulk matrix. The opposite is true for trapped deuterium, and the volumetric strain associated with segregated deuterium can be partially cancelled or "contrast matched" at low deuterium concentration. We believe this is the case in Fig. 3.

The original analytical cross section published by Heuser *et al.* assumed a dilute mixture of solute-decorated dislocations and included a cylindrical form factor characterized by a radius $R$ and length $L$ [3, 4],

$$\frac{d\Sigma}{d\Omega}(Q) = \frac{\pi b_S^2 \rho_S^2}{\rho_d} \frac{1}{Q} exp\left(\frac{-Q^2R^2}{4}\right)\left[\frac{2}{\pi}\tan^{-1}(QL)\right] \quad , \qquad [1]$$

where $\rho_S$ is the measured excess or trapped solute number density averaged over the entire sample volume and is given by $\rho_S = \rho_T - \rho_B = \pi R^2 L N_d C_S$ with $C_s$ equal to the local interstitial solute number density trapped within the near-dislocation environment [3] (see below), $\rho_d$ is the volume-average dislocation density, in units of line length per unit volume, given by $\rho_d = LN_d$ with $N_d$ defined as the number of dislocation defects per unit volume, and $Q$ is the wave-vector transfer. This analytical result is defined by a $Q$-independent amplitude or pre-factor and a $Q$-dependent shape function. The $Q$-dependent function represents a pure $Q^{-1}$ response for a zero-radius, infinitely-long line defect modified to account for non-zero radius $R$ (the so-called Guinier radius [6]) and finite cylinder length $L$ [3]. The development of Eqn. 1 ignored the volumetric dilatation associated with solute segregation at dislocations and any effect this may have on the observed SANS response. Maxelon *et al*. took into account the volumetric dilatation associated with solute segregation and developed a modified analytical cross section for $QL$>>1 (such that $\tan^{-1}(QL) \rightarrow \pi/2$) given by [5],

$$\frac{d\Sigma}{d\Omega}(Q) = \pi \frac{\rho_S^2}{C_S^2 \rho_d} \left( \frac{N_{Pd} b_{Pd}}{f} + \delta N_{Pd} b_S - N_{Pd} b_{Pd} \right)^2 \frac{1}{Q} exp\left( \frac{-Q^2 R^2}{4} \right), \quad [2]$$

where $f$ is the volumetric dilatation at the dislocation defect associated with solute segregation (set to $f$ = 1.12, the value corresponding to hydride/deuteride phase formation in Pd, by Maxelon *et al.* [5]), $\delta$ is the local or trapped solute concentration (set to $\delta$ = 0.6 [solute]/[Pd], the value corresponding to the hydride/deuteride phase in Pd, by Maxelon *et al*. [5]), and $N_{Pd}$ is the bulk Pd atomic number density. The pre-factor originally developed by Heuser *et al*. and that developed by Maxelon *et al*. are equivalent for $f \rightarrow 1$ since $C_s \equiv \delta N_{Pd}$. This is consistent with the original approximation by Heuser *et al*. that local solute segregation at dislocation does not perturb the Pd lattice (i.e., $f$ = 1). Note that the volumetric expansion associated with the interstitial solute in bulk (i.e., Vegard's law for hydrogen/deuterium in Pd) is ignored in Equation 2. This is a valid assumption for the low bulk concentrations, ~$10^{-3}$ to $10^{-2}$ [solute]/[Pd].

The approach we use here is to fit the data with the $Q$-dependent function given by Eqn. 1 with a constant amplitude pre-factor given by Eqn. 2, which we defined as $A$ for data fitting purposes. The use of the $Q$ dependence given by Eqn. 1 avoids the $QL$>>1 assumption, while the use of the amplitude pre-factor given by Eqn. 2 correctly accounts for the local volumetric strain associated with solute segregation. We refer to this combined cross section as the "analytical model." The fit of the analytical model to the net absolute $PdH_{0.0013}$ measurements at 15, 100, and 200K are shown in Figure 4. The net absolute cross section is defined as the difference between the with-hydrogen and zero-concentration deformed Pd reference sample. This subtraction eliminates incoherent background from Pd, which is temperature dependent, and weak scattering from dislocation defects [3, 4, 7]. The SANS response of the $PdH_{0.0013}$ sample shows very little temperature dependence (the 100 and 200K curves in Fig. 4 are shifted upward by one and two factors of $e$, respectively). The fitting parameters $A$, $R$, and $L$ are listed in Table 1. We include the 15 and 100K $PdD_{0.00084}$ data in Table 1 as well, even though the net data are poorly resolved in this case (uncertainties in $A$ and $R$ are of order 100%). In addition, the 295 K-data from sample SC14 ($PdD_{0.0072}$) of Ref. 4 is included in Table 1. This was a single crystal Pd sample deformed by hydride cycling and measured at equilibrium with respect to the $D_2$ gas phase at room temperature [4].

## 3. Analysis

The use of the analytical model to determine the local interstitial solute concentration trapped at dislocations $\delta$, the quantity of interested to support our recent incoherent inelastic neutron scattering (IINS) work [13], requires a value of $f$—Maxelon *et al.* assumed $f$=1.12, the known bulk hydride/deuteride volumetric expansion [14]. We do not make this assumption *a priori*. The analytical model pre-factor $A$ in Eqn. 2 can be rewritten after substituting for $C_S = \rho_S(\pi R^2 \rho_d)^{-1}$ as,

$$A = 2(\pi R^2)^2 \rho_d \left[ N_{Pd} b_{Pd} \left( \frac{1}{f} - 1 \right) + \frac{\rho_S b_S}{(\pi R^2)\rho_d} \right]^2 . \quad [3]$$

This is a quadratic equation in $\rho_d$ yielding two solutions for the solute-decorated dislocation density. Note the two other parameters in Eqn. 3 are known; $R$ from the fit of the $Q$-dependent form factor of the analytical model and $\rho_S$ from the solubility measurement. An alternative data display to determine $R$, sometimes referred to as a modified Guinier plot, is shown in Figure 5 for the net $PdH_{0.0013}$ measurements. A linear fit to the high-$Q$ region of $\ln(Q^* d\Sigma/d\Omega)$ versus $Q^2$ yields the radius $R$ of the analytical model. This display demonstrates the applicability of the Guinier modifier term since a linear response with non-zero slope should be observed at high $Q$. Fits to the linear, high-$Q$ portion of these data resulted in nearly identical Guinier radii with comparable error as listed in Table 1. The two solutions to Eqn. 3 for the net $PdH_{0.0013}$ data are shown in Figure 6 with $f$ as the independent variable. The corresponding values of $\delta$ are plotted in Fig. 7, again with $f$ as the independent variable. Similar analysis ($\delta$ vs. $f$) is shown in Fig. 8 for the three Pd-deuterium samples (15 and 100K $PdD_{0.00084}$, and 295 K $PdD_{0.0072}$). Note that the different $\delta(f)$ behaviors of the hydrogen- and deuterium-loaded samples in Figs. 7 and 8 are the result of the sign change of the solute scattering length.

Figures 6-8 represents all possible solutions for $\rho_d$ and $\delta$ that satisfy the constraint of the measured SANS pre-factor $A$ and shape function parameter $R$. We must rely on known physical properties and physical insight for the selection of $\rho_d$, and hence $\delta$ from these solutions. First, note low $\rho_d$ values correspond to a high local concentration $\delta$ and vice versa. This is consistent with a fixed total trapped solute concentration $\rho_S$ that must exist under the assumption that no hydrogen is lost from the sample during the low temperature SANS measurements. The one relevant physical property of the Pd-H system we can employ is Vegard's law for the hydride phase in Pd [14],

$$\frac{\Delta v}{\Omega} = f - 1 = 0.19\,\delta \quad , \qquad [4]$$

where $\Delta v/\Omega$ is the concentration-dependent volumetric expansion at room temperature. The mapping of Eqn. 4 onto the $\delta$ vs. $f$ dependence in Fig. 7 represents the application of a second constraint, in addition to that provided by the measured $A$-$R$ combination, to the solutions $\delta^l$ and $\delta^h$. The intersection of Eqn. 4 with either of the $\delta^l$ or $\delta^h$ branches represents local conditions ($\delta$–$f$ combinations) at dislocation defects that satisfy Eqn. 3 for the dislocation density via $\rho_d = \rho_S(\delta N_{Pd}\pi R^2)^{-1}$ and Vegard's law for the known volumetric dilatation of the hydride phase in Pd. It is immediately clear that the $\rho_d^h$ solutions to Eqn. 3 are unphysical since the corresponding $\delta^l$ values cannot satisfy Vegard's law. The intersection points from Fig. 7 are listed in Table 2 together with the corresponding dislocation density values $\rho_d^l$.

One caveat in this analysis is Eqn. 4 represents the room temperature behavior and does not account for thermal contraction of the lattice upon cooling. The effect temperature can be estimated using the linear expansion coefficient of Pd (11.8 x $10^{-6}$ 1/K; the corresponding coefficient for Pd hydride is not known to the best of our knowledge). We apply this correction at 15, 100, and 200 K for the $PdH_{0.0013}$ sample and list a second set of points $\delta'$–$f'$ in Table 2. Consideration of Fig. 7 and Table 2 indicates a high-concentration phase ($\delta$~0.6±0.1) at $f$~1.1 in $PdH_{0.0013}$, consistent with the known volumetric dilatation of $PdH_{0.6}$. This is also consistent with the assumptions initially used by Maxelon *et al*. [5]. The dislocation density $\rho_d$~4x$10^{10}$ $cm^{-2}$ corresponding to this phase is the smallest root of Equation 3. A second caveat is the assumption that Eqn. 4 holds exactly at dislocations. It is likely

the tensile strain regions associated with the near-dislocation environment will have an effect on the $\Delta v/\Omega$ ($\delta$) dependence. We do not expect this to be a dominating effect, however, since the dilatation associated with hydride formation is significantly larger than those related to the edge dislocation elastic strain field [15].

The uncertainties in both $\rho_d$ and $\delta$ for the $PdH_{0.0013}$ data are high, even though the relative errors in *A* and *R* are ~2% and ~5%, respectively. The reason for this is the propagation of error in the solutions to Eqn. 3, in particular the propagation of the error in *R*. We believe the $\rho_d^l - \delta^h$ combination for the $PdH_{0.0013}$ data is the correct representation of the local solute trapping parameters at dislocation defects for the following reasons. First, the magnitude of the dislocation density ($\rho_d$~$10^{10}$ $cm^{-2}$) corresponds to that associated with moderately deformed metals, as is the case here. Second, the local solute concentration corresponds to the known non-stoichiometric hydride phase in Pd (i.e., $PdH_{0.6}$) expected for a volumetric dilatation of *f*~1.1. Most importantly, the $\rho_d^l - \delta^h$ combination satisfies the constraints of both Vegard's law (Eqn. 4) and the SANS measurement via *A* and *R* fitting. Finally, the presence of the hydride phase in deformed Pd at low temperature and low hydrogen concentration was recently confirmed in IINS measurements of the hydrogen vibrational density of states [13]. This is discussed in the next section.

We perform similar analysis for the 15 K and 100 K $PdD_{0.00084}$ data presented here and the 295 K $PdD_{0.0072}$ data from Reference 4 in Figure 8. (The application of the temperature correction to Vegard's law for the $PdD_{0.00084}$ results is unwarranted given the large uncertainties that exist in these data sets.) The local solute concentrations satisfying Vegard's law (the intersection points in Fig. 8 with the $\delta^h$ branches) are listed in Table 2 together with the corresponding dislocation density values $\rho_d^l$. The 295 K $PdD_{0.0072}$ intersection point of $\delta(f)$ with Vegard's law is consistent with $PdD_{0.6}$ formation at dislocations in this sample. The 15 K and 100 K $PdD_{0.00084}$ intersection points indicate deuteride phase formation in the local dislocation trapping environment, but at lower solute concentration.

## 4. Discussion and Summary

A few statements can be made regarding the values listed in Table 2. The local or trapped concentration in the $PdD_{0.00084}$ measurements are approximately one fifth that of the $PdH_{0.0013}$ sample, indicating the deuterium-containing sample was further from solute saturation of the dislocation trapping sites. While this is consistent with the lower total solute concentration, the low $\delta$–*f* combination must be considered in the context of the very large uncertainties associated with the $PdD_{0.00084}$ data. The weak scattering response and corresponding large fitting parameter errors for this sample are due in part to the contrast matching condition referred to in Section 2. The relatively small $\delta$~0.1 [D]/[Pd] value is consistent with the weak, but not zero, net scattering observed in the $PdD_{0.00084}$ SANS measurement. The 295 K $PdD_{0.0072}$ data demonstrates this effect is overcome at large deuteride concentrations.

Large net scattering was observed in the original room temperature $PdD_{0.0072}$ SANS measurements [4]. Analysis using the current analytical model results in a trapped solute concentration similar to that observed for the $PdH_{0.0013}$ sample ($\rho_d^l - \delta$ combination, Table 2). However, the dislocation density is a factor of two higher. This is consistent with the larger total solute concentration of the $PdD_{0.0072}$ sample leading to a greater number of solute-decorated dislocations with saturated local concentration ($\delta$~0.5). Thus, an increase in the total solute concentration decorates more dislocations without a significant increase in the local concentration. This is expected since the Pd-H (-D) system, even locally near dislocations, cannot easily go beyond $\delta$~0.6 at chemical potential or fugacity values

associated with $H_2$ ($D_2$) gas exposure, except possibility at inordinately high pressure. One related point with regard to the $PdD_{0.0072}$-$PdH_{0.0013}$ comparison is that the Guinier radius of the former is larger (Table 1)—we believe this difference is real and indicative of the growth Pd deuteride phase to larger radii about the dislocation defects. We therefore attribute both the larger dislocation density and larger Guinier radius of the $PdD_{0.0072}$ measurement to greater total solute concentration.

Weak temperature dependence is observed in the $PdH_{0.0013}$ and $PdD_{0.00084}$ SANS responses. A slight decrease in the Guinier radius $R$ was observed (Table 1) as the measurement temperature increases for the $PdH_{0.0013}$ sample. Although the $R$-values for this sample are within the quoted uncertainty, this increase is consistent with the de-trapping of solutes atoms at higher temperature. The same trend in dislocation density is observed with increasing temperature, again consistent with a smaller number of solute-decorated dislocations.

The SANS measurements presented here have been performed in part to support recent IINS measurements of deformed polycrystalline $PdH_{0.0008}$ [13]. IINS is a neutron spectroscopy technique sensitive to the vibrational density of states (VDOS). In the case of the Pd-H system, the observed optic modes are due solely to the presence of hydrogen since Pd has just a single atom in the primitive cell. The first harmonic of the hydrogen optic modes occurs over an energy transfer range of ~40 to 100 meV [13]. The measured spectra over this energy range are proportional to the number of phonon states per unit energy that the hydrogen atoms can occupy. An energy shift or softening was observed from the hydrogen optic mode in the measured VDOS at 4 K. This softening was attributed to trapped hydrogen forming the hydride phase, with associated volumetric dilatation, for several reasons. First, the measured VDOS matched the recorded spectra for Pd hydride ($PdH_{0.63}$) very well, including the position of the primary peak and the high-energy shoulder typically attributed to dispersion on the longitudinal optic mode [13]. Second, the low temperature and low hydrogen concentration conditions of IINS measurement dictated that a significant fraction of all hydrogen solute impurities were trapped in the heavily deformed Pd matrix—presumably a requirement for hydride formation. Third, the softening of the hydrogen optic mode was *reversed* upon warming to ambient temperature while maintaining equilibrium with respect to the $H_2$ gas phase. In fact, the room-temperature VDOS matched the measured spectra for the solid solution $\alpha$ phase of well-annealed $PdH_{0.015}$, including the position of the primary peak. Thus, the hydride→solid solution Pd phase transformation was hypothesized to occur *at dislocations* upon warming from 4 K to 295 K. A direct measurement of the locally-trapped hydrogen concentration, $\delta$ here, under similar temperature-solute concentration conditions is important since it represents additional and independent proof of hydride phase formation at dislocations. The trapped hydrogen concentration ($\delta$~0.5) and associated volumetric dilatation ($f$~1.1) obtained here for $PdH_{0.0013}$ at low temperature is consistent with Pd hydride and therefore supports the IINS-based hypothesis.

The $PdD_{0.00084}$ data at 15 K may or may not support to the IINS measurements since a low $\delta$ value was obtained via the application of Vegard's law in Figure 8. The uncertainties in $\delta$ are very high, however, and this limits the utility of these data. Furthermore, an isotopic effect is known to exist in face-centered cubic metals that results in lower deuterium solubility compared to hydrogen at identical fugacity [16]. A similar argument will hold for the trapped solute relative to the bulk solute concentration. While the 353 K solubility measurements of Maxelon *et al*. [5] and our 295 K measurements (Fig. 1) demonstrate that the isotope effect in deformed Pd is small at room temperature and above, it is expected to become larger as the system temperature is reduced. We therefore believe the solubility isotope effect could explain the lower $\delta$ values observed here for $PdD_{0.00084}$ at low temperature. In any event, $\delta$~0.1 does represent phase separation since the terminal solid-solution solubility will be effectively zero at low temperature.

The following statements summarize this work:

1. The observed SANS response from deformed single crystal $PdH_{0.0013}$ is consistent with the formation of a hydride phase ($PdH_{0.5}$) at dislocations, as is a re-analysis of the deformed single crystal $PdD_{0.0072}$ data from Reference 4. The volumetric dilatation associated with hydride (deuteride) formation at dislocations is consistent with that expected from Vegard's law for the Pd-hydride system ($f$~1.1).

2. The observed SANS response from deformed single crystal $PdD_{0.00084}$ is poorly resolved; the increase in neutron scattering length associated with deuteride formation partially offsets the volumetric dilatation of the Pd lattice associated with phase separation at low solute concentration. The $PdD_{0.00084}$ data are consistent with phase separation (i.e., deuteride formation) at dislocations, but at low local concentration and low local volumetric dilatation. However, conclusive statements regarding the local trapping conditions from these data are not possible given the very large uncertainty in $\rho_d$ and $\delta$ derived from the analysis.

3. The trapped hydrogen concentration and volumetric dilatation at low temperature derived from the $PdH_{0.0013}$ SANS data presented here support the hypothesis of hydride formation at dislocations. This adds independent confirmation of recent IINS measurements under similar hydrogen concentration-temperature conditions in deformed Pd.

Acknowledgements

This work was supported by the NSF under Grant Number DMR-0804810. The SANS measurements were performed at Oak Ridge National Laboratory's High Flux Isotope Reactor. This facility is sponsored by the Scientific User Facilities Division, Office of Basic Energy Sciences, United States Department of Energy. The TEM images were supplied by I. Robertson, J. Fenske, and V. McCreary (Univ. Illinois) and this is gratefully acknowledged. The TEM work at the Univ. of Illinois was supported by the U.S. DOE Office of Basics Sciences as part of the Center for Defect Physics under Award Number DE-AC05-00OR22715. In addition, the TEM work was carried out in part in the Frederick Seitz Materials Research Laboratory Central Facilities, University of Illinois, which are partially supported by the U.S. Department of Energy under grants DE-FG02-07ER46453 and DE-FG02-07ER46471.

References


1. R. Kirchheim, X.Y. Huang, H.-D. Carstanjen, and J.J. Rush, *Chemistry and Physics of Fracture*, NATO ASI Series, Series E. No. 130, FRG, p. 580 (1987).

2. H.-D. Carstanjen, X.Y. Huang, W. Kieninger, R. Kirchheim, J. Rush, T. Udovic, J. Glinka, and A. Petry, *Z. Physik Chem. Neue Folge* **163**, 203 (1989).

3. B.J. Heuser, J.S. King, G.C. Summerfield, F. Boue, and J.E. Epperson, *Acta metall. Mater*., **39**, 2815 (1991).

4. B.J. Heuser and J.S. King, *J. Alloys Compounds*, **261**, 225 (1997).

5. M. Maxelon, A. Pundt, W.Pyckhout-Hintzen, J. Barker, and R. Kirchheim, *Acta mater*., **49**, 2625 (2001).

6. A. Guinier and G. Fournet, *Small Angle Scattering of X-rays*, Wiley, New York (1955).

7. B.J. Heuser, *Ph.D. Dissertation*, University of Michigan, Ann Arbor, MI, 1990.

8. T.B. Flanagan, J.F. Lynch, J.D. Clewley, and B. von Turkovich, *J. Less-Common Metals*, **49**, 13 (1976).

9. H. Ju, B.J. Heuser, D.R. Trinkle, V. McCreary, J.A. Fenske, and I.M. Robertson, submitted *J. Phys.: Conds. Matter.*

10. F. Fromm and H. Jehn, *Bull. Alloy Phase Dia*., **5**, 325 (1984).

11. K.C. Littrell, K.M. Atchley, G. Cheng. Y.B. Melnichenko, and G.D. Wignall, *Neutron News*, **19**, 20, (2008).

12. J. Völkl and G. Alefeld, *Hydrogen in Metals I: Basic Properties, Topics in Applied Physics*, Eds. G. Alefeld and J. Volkl, Springer-Verlag, Berlin, 1978, p. 321.

13. B.J. Heuser, T.J. Udovic, H. Ju, *Phys. Rev. B*, **78** 214101 (2008).

14. H. Peisl, *Hydrogen in Metals I: Basic Properties, Topics in Applied Physics*, Eds. G. Alefeld and J. Volkl, Springer-Verlag, Berlin, 1978, p. 70.

15. B.J. Heuser, H. Ju, D.R. Trinkle, and T.J. Udovic, *Effects of Hydrogen on Materials*, Proceedings of the 2008 International Hydrogen Conference, Eds.: B. Somerday, P. Sofronis, and R. Jones, ASM International, Materials Park, OH, 2009, p. 464.

16. R. Lasser, *Tritium and Helium-3 in Metals*, Springer Series in Materials Science 9, Springer-Verlag, Berlin, 1989.

Table 1. Sample solubility measurement values and SANS fitting parameters.

| Sample | $T$ [K] | $\rho_T$ [x$10^{19}$ cm$^{-3}$] | $\rho_B$ [x$10^{19}$ cm$^{-3}$] | $A$ [x$10^{4}$ cm$^{-2}$] | $R$ [Å] | $L$ [Å] |
|---|---|---|---|---|---|---|
| $PdH_{0.0013}$ | 15 | 9.10 | 5.37 | 1.44±0.03 | 8.9±0.4 | 56±4 |
| $PdH_{0.0013}$ | 100 | 9.10 | 5.37 | 1.54±0.04 | 9.0±0.4 | 59±3 |
| $PdH_{0.0013}$ | 200 | 9.10 | 5.37 | 1.54±0.05 | 8.3±0.5 | 48±3 |
| $PdD_{0.00084}$ | 15 | 5.67 | 2.48 | 0.3±0.3 | 8±7 | 10±11 |
| $PdD_{0.00084}$ | 100 | 5.67 | 2.48 | 0.3±0.2 | 9±5 | 12±10 |
| $PdD_{0.0072}$* | 295 | 48.6 | 37.4 | 9.0 | 11 | 60 |

* Measurement from Reference 4. The original data from this publication was not retrievable and error propagation was not possible.

Table 2. Local volumetric dilatation, dislocation density, and trapped solute concentration values corresponding to the application of Vegard's law locally at dislocation defects (intersection points in Figs. 7 and 8).

| Sample | $T$ [K] | $f$ | $f'$ | $\rho_d^l$ [x$10^{11}$ cm$^{-2}$]† | $\delta$ [solute]/[Pd]† | $\delta'$ [solute]/[Pd]† |
|---|---|---|---|---|---|---|
| $PdH_{0.0013}$ | 15 | 1.095 | 1.091 | 0.44±0.4 | 0.50±0.5 | 0.52±0.5 |
| $PdH_{0.0013}$ | 100 | 1.10 | 1.097 | 0.41±0.4 | 0.52±0.5 | 0.54±0.5 |
| $PdH_{0.0013}$ | 200 | 1.12 | 1.12 | 0.39±0.6 | 0.62±0.9 | 0.63±0.9 |
| $PdD_{0.00084}$ | 15 | 1.022 | ----- | 21±384 | 0.1±2 | ----- |
| $PdD_{0.00084}$ | 100 | 1.016 | ----- | 25±480 | 0.1±1 | ----- |
| $PdD_{0.0072}$* | 295 | 1.095 | ----- | 1 | 0.5 | ----- |

* Measurement from Reference 4. The original data from this publication was not retrievable and error propagation was not possible.

† Two significant digits are shown for the $PdH_{0.0013}$ data to illustrate trends with respect to temperature despite lack of corresponding error precision.

Figure Captions

Figure 1. Transmission electron microscopy images of deformed Pd after room-temperature cold working (a) and after subsequent hydride cycling (b). The cellular substructure after cold working is evident in (a); hydride cycling then populates the cell interiors with additional dislocations defects in (b).

Figure 2. Solubility enhancement ratio versus total solute concentration in deformed single crystal Pd. Four different measurements are shown: a continuous series of hydrogen in the single crystal sample (solid boxes); deuterium in the single crystal sample corresponding to $PdD_{0.00084}$ and $PdD_{0.0072}$ SANS measurements (solid diamonds); and hydrogen in the single crystal sample corresponding to the $PdH_{0.0013}$ SANS measurement (open box). The solid line is drawn as a guide.

Figure 3. Radial-averaged absolute macroscopic differential scattering cross section versus wavevector transfer measured at 15 K for the three deformed single crystal Pd samples identified. The response from the $PdD_{0.00084}$ measurement is poorly resolved above the zero-hydrogen deformed single crystal reference sample.

Figure 4. Net absolute macroscopic differential scattering cross section for the $PdH_{0.0013}$ measurements at the temperatures listed. The 100K and 200K measurements have been shifted upward by factors of $e$ and $2e$, respectively, for clarification. The data at each temperature has been fit with the analytical model discussed in the text. The three fitting parameters determined in the fit, $A$, $R$, and $L$, are listed in Table 1.

Figure 5. Modified Guinier plot for the $PdH_{0.0013}$ measurements illustrating the effect of the Guinier modifier term on pure $1/Q$ response. Best fits to the linear high-$Q$ portion of these data yield Guinier radii equivalent to the fits shown in Figure 4. The 100K (open boxes) and 200K (open diamonds) data have been shifted by factors of $e$ and $2e$, respectively, from the 15K (open circles) data.

Figure 6. Dislocation density solutions $\rho_d$ to Eqn. 3 for the for the $PdH_{0.0013}$ measurements at the temperatures shown (100K not labeled). The positive and negative roots are shown as solid and dotted lines, respectively. A break in each solution data set is intentionally present for clarification.

Figure 7. Local or trapped hydrogen concentration $\delta$ for the $PdH_{0.0013}$ measurements at the temperatures shown. The $\delta$ values associated with the $\rho_d$ solutions (positive root—solid lines; negative root—dotted lines) are shown, as discussed in the text. Vegard's law for the hydrogen concentration dependence on volumetric dilatation for Pd hydride at 295K (Eqn. 4) is shown as a solid line. The intersection of Vegard's law with $\delta$ curves indicates points for each measurement that satisfy the constraint of i) the known Pd hydride volumetric lattice expansion dependence

on concentration and ii) the observed SANS intensity via the fitted values of $A$ and $R$. These intersections points are listed in Table 2.

Figure 8. Local or trapped hydrogen concentration $\delta$ for the 15K-$PdD_{0.00084}$, the 100K-$PdD_{0.00084}$, and the 295K-$PdD_{0.0072}$ measurements. The $\delta$ values associated with the $\rho_d$ solutions (positive root—solid lines; negative root—dotted lines) are shown, as discussed in the text. Vegard's law for the hydrogen concentration dependence on volumetric dilatation for Pd hydride at 295K (Eqn. 4) is shown as a solid line. The intersection of Vegard's law with $\delta$ curves indicates points for each measurement that satisfy the constraint of i) the known Pd hydride volumetric lattice expansion dependence on concentration and ii) the observed SANS intensity via the fitted values of $A$ and $R$. These intersections points are listed in Table 2.

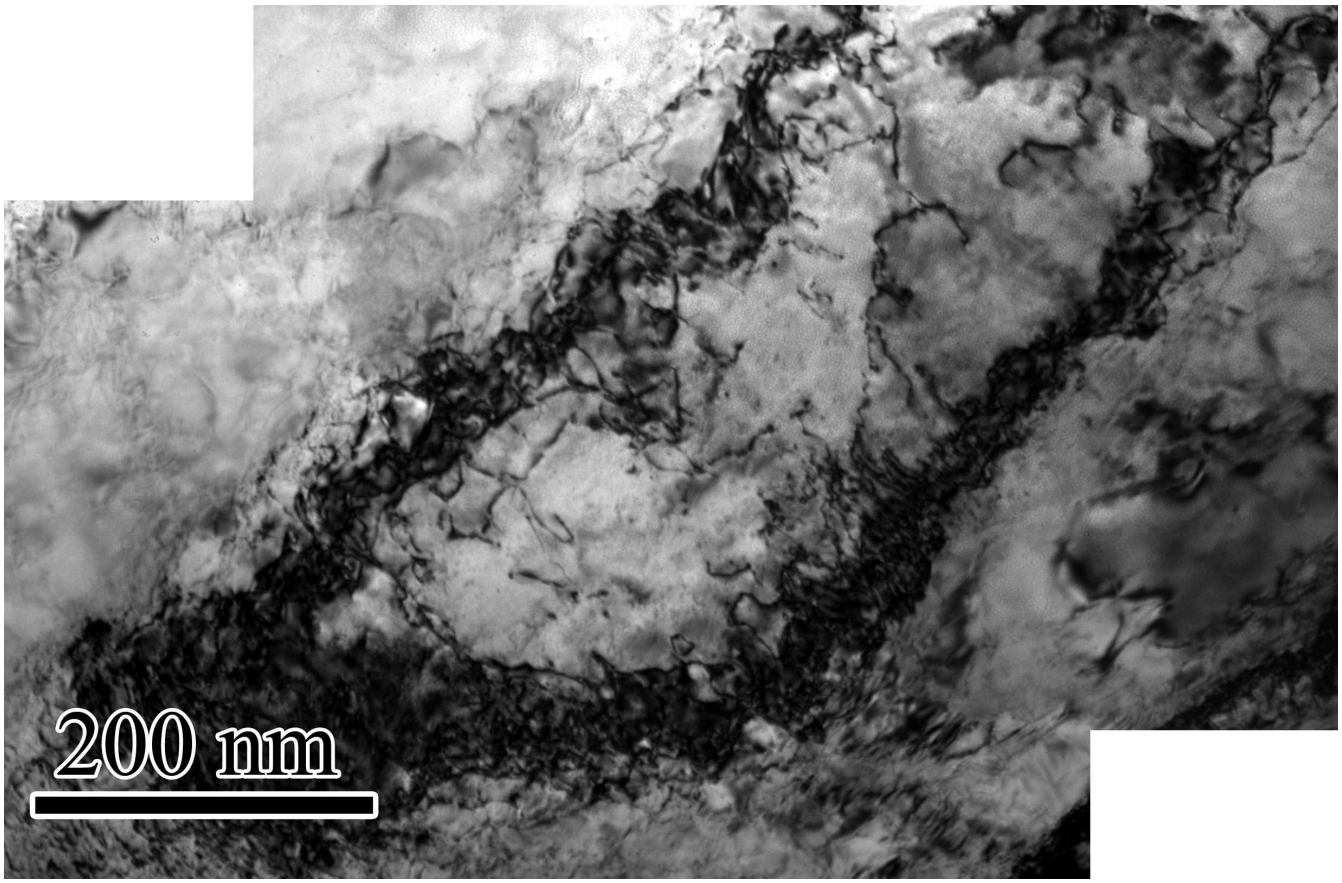


Figure 1a BY11279 31JAN2011

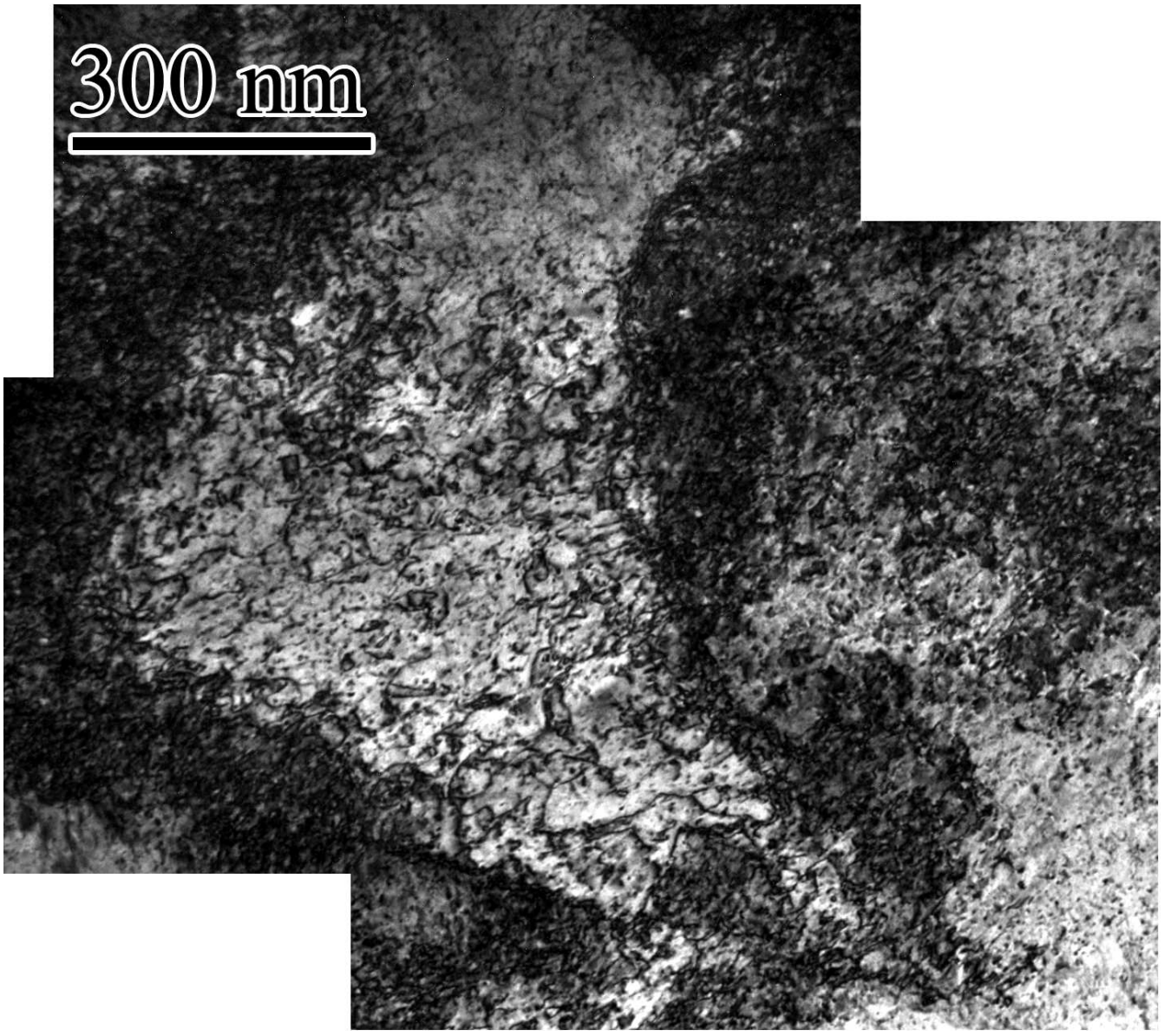


Figure 1b BY11279 31JAN2011

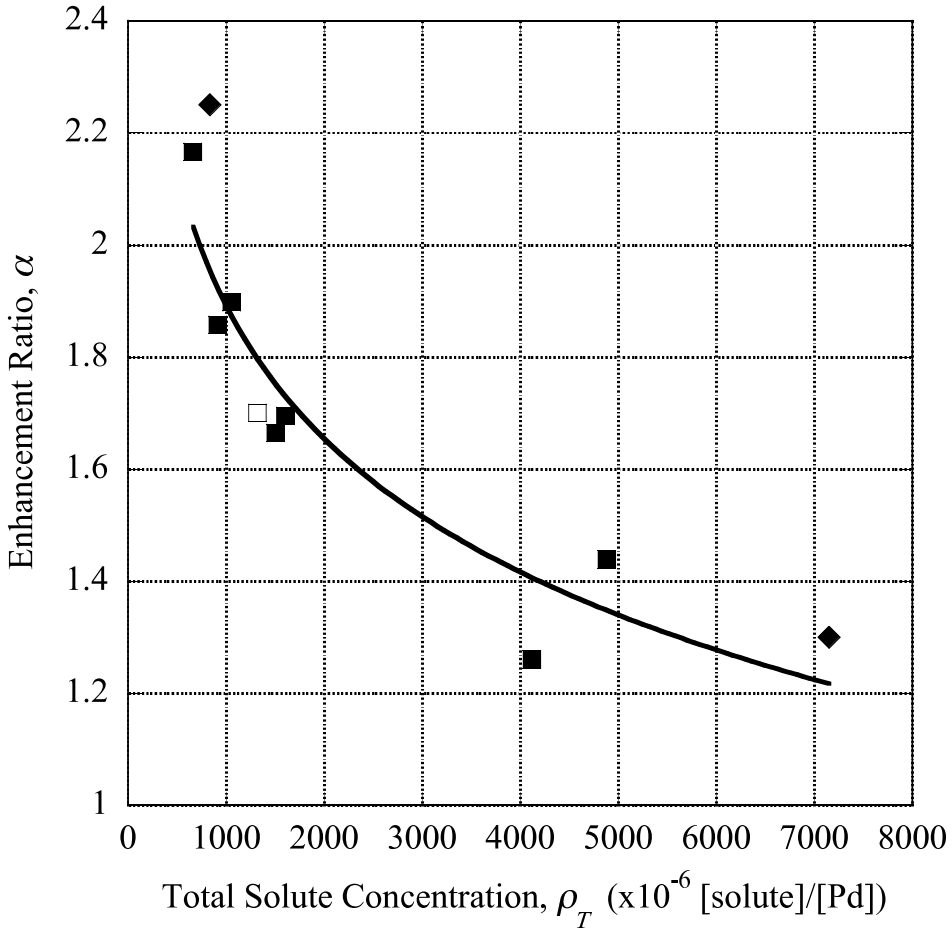


Figure 2 BY11279 31JAN2011

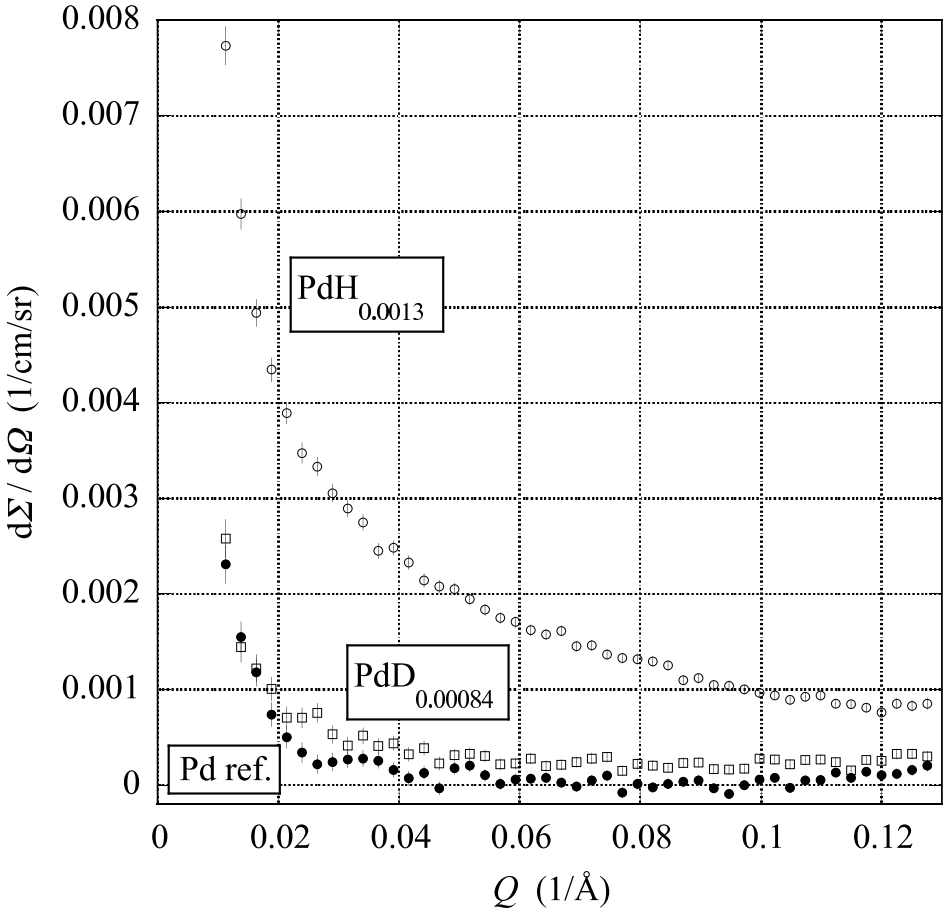


Figure 3 BY11279 31JAN2011

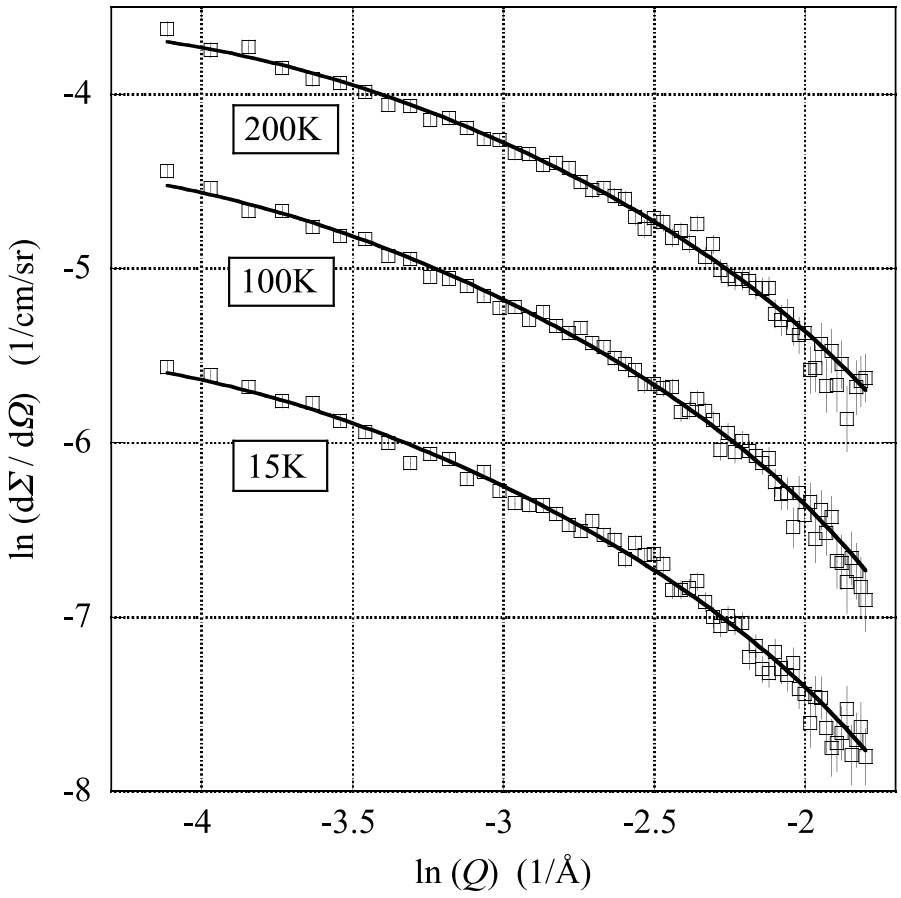


Figure 4 BY11279 31JAN2011

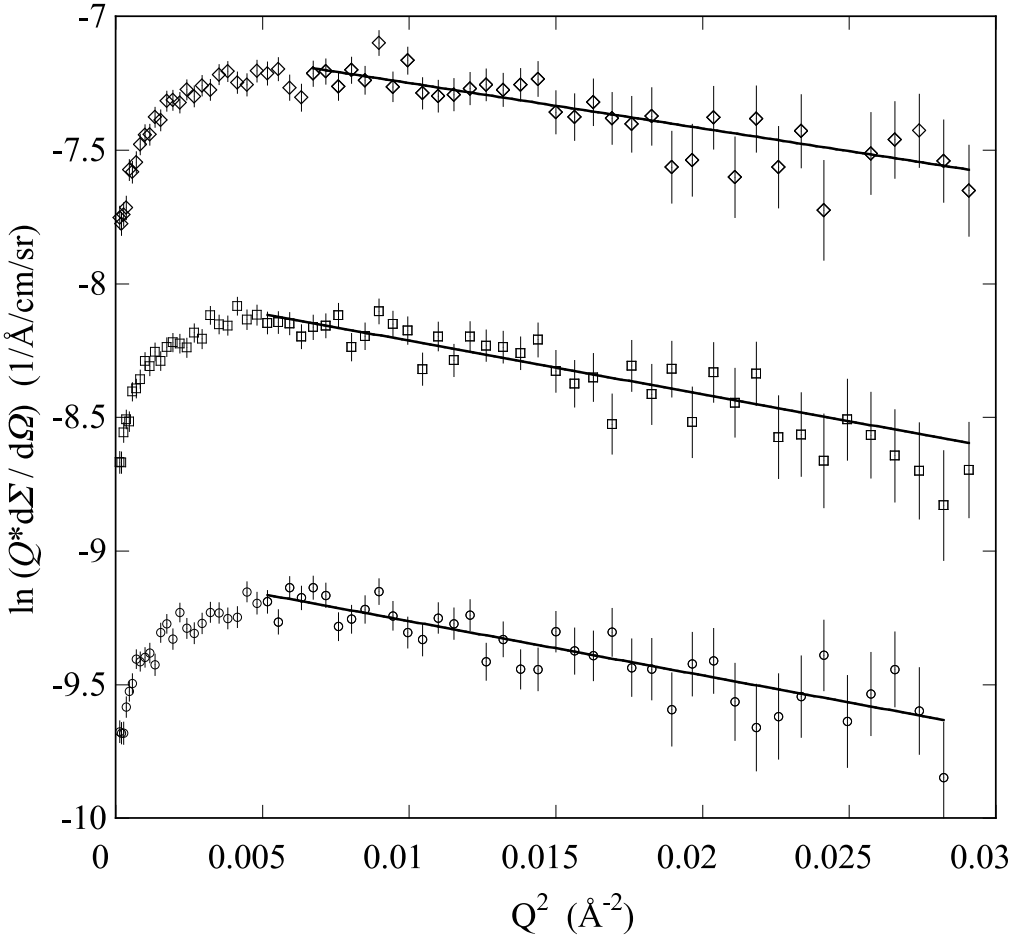


Figure 5 BY11279 31JAN2011

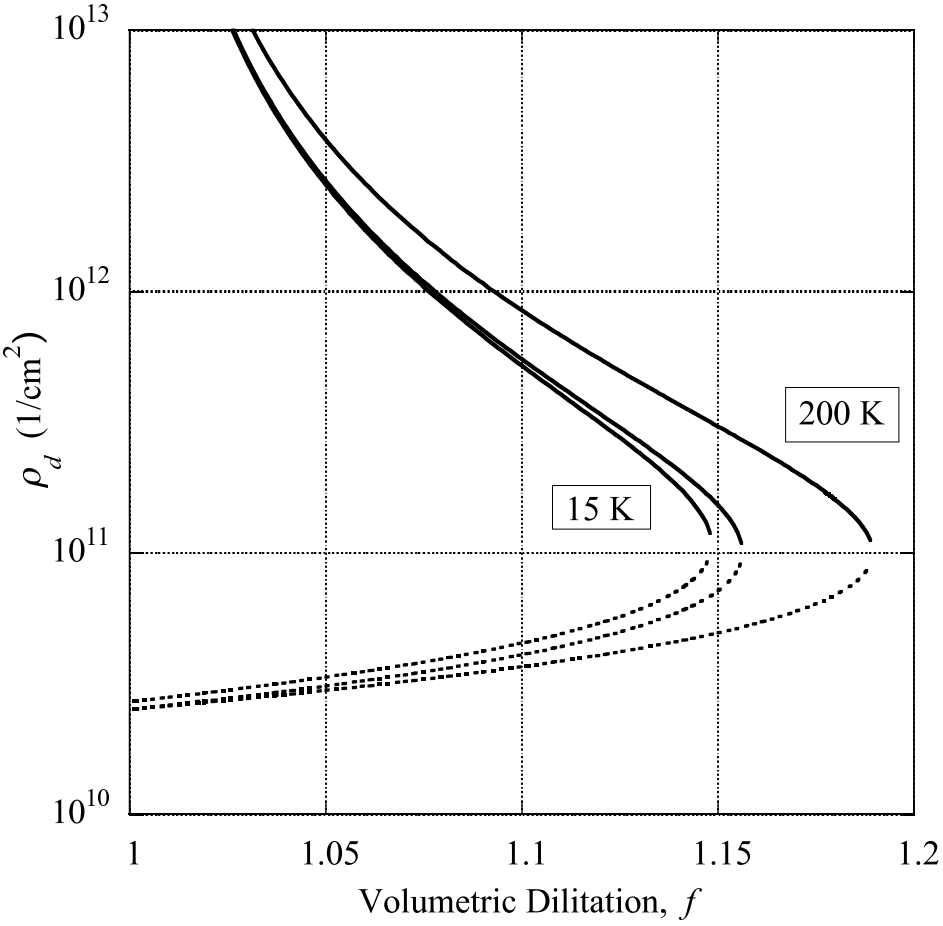


Figure 6 BY11279 31JAN2011

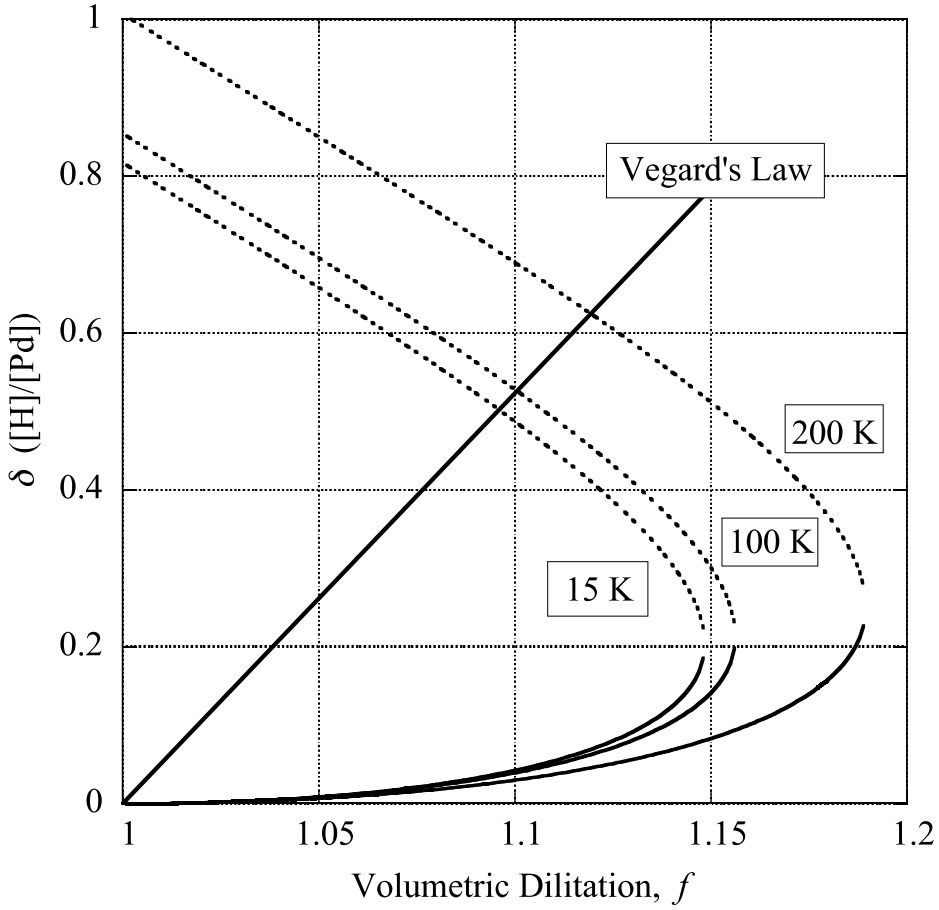


Figure 7 BY11279 31JAN2011

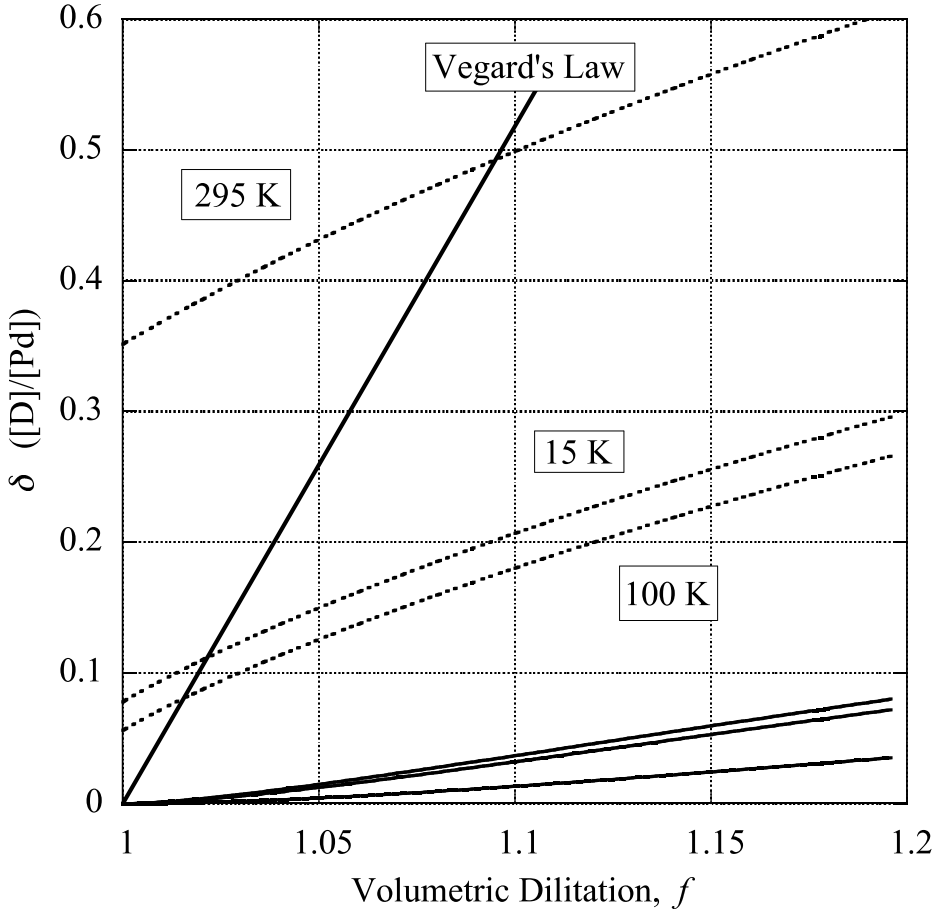


Figure 8 BY11279 31JAN2011